TISSUE ENGINEERING: Part A
Volume 21, Numbers 5 and 6, 2015

DOI: 10.1089/ten.tea.2013.0789

Osseointegrative Properties of Electrospun Hydroxyapatite-Containing Nanofibrous Chitosan Scaffolds

Michael E. Frohbergh, PhD,[1,2] Anya Katsman, MD,[3] Mark J. Mondrinos, PhD,[4] Collin T. Stabler, BS, MSc,[5] Kurt D. Hankenson, PhD,[6] Jeffrey T. Oristaglio, PhD,[7] and Peter I. Lelkes, PhD[1,5]

Our long-term goal is to develop smart biomaterials that can facilitate regeneration of critical-size craniofacial lesions. In this study, we tested the hypothesis that biomimetic scaffolds electrospun from chitosan (CTS) will promote tissue repair and regeneration in a critical size calvarial defect. To test this hypothesis, we first compared *in vitro* ability of electrospun CTS scaffolds crosslinked with genipin (CTS-GP) to those of mineralized CTS-GP scaffolds containing hydroxyapatite (CTS-HA-GP), by assessing proliferation/metabolic activity and alkaline phosphatase (ALP) levels of murine mesenchymal stem cells (mMSCs). The cells' metabolic activity exhibited a biphasic behavior, indicative of initial proliferation followed by subsequent differentiation for all scaffolds. ALP activity of mMSCs, a surrogate measure of osteogenic differentiation, increased over time in culture. After 3 weeks in maintenance medium, ALP activity of mMSCs seeded onto CTS-HA-GP scaffolds was approximately two times higher than that of cells cultured on CTS-GP scaffolds. The mineralized CTS-HA-GP scaffolds were also osseointegrative *in vivo*, as inferred from the enhanced bone regeneration in a murine model of critical size calvarial defects. Tissue regeneration was evaluated over a 3 month period by microCT and histology (Hematoxylin and Eosin and Masson's Trichrome). Treatment of the lesions with CTS-HA-GP scaffolds induced a 38% increase in the area of *de novo* generated mineralized tissue area after 3 months, whereas CTS-GP scaffolds only led to a 10% increase. Preseeding with mMSCs significantly enhanced the regenerative capacity of CTS-GP scaffolds (by $\sim$3-fold), to 35% increase in mineralized tissue area after 3 months. CTS-HA-GP scaffolds preseeded with mMSCs yielded 45% new mineralized tissue formation in the defects. We conclude that the presence of HA in the CTS-GP scaffolds significantly enhances their osseointegrative capacity and that mineralized chitosan-based scaffolds crosslinked with genipin may represent a unique biomaterial with possible clinical relevance for the repair of critical calvarial bone defects.

Introduction

Craniofacial reconstruction involves the repair or replacement of bones malformed or fractured due to a congenital defect or a traumatic injury. A defect is considered of critical size when it does not spontaneously heal on its own[1] and requires intervention. Surgical options available to restore critical size defects traditionally have included autografts, tricalcium phosphate-containing biomaterials that mimic some features of hydroxyapatite (HA), and inert metallic compounds. However, because of the various complications associated with each of these components, allogeneic materials are emerging as a new strategy. In the past, treatments of defective or injured nonload-bearing cranial and maxillofacial bones have primarily focused on replacement rather than regeneration.

In the United States alone, craniofacial defects affect over 250,000 children annually.[2] Such birth defects frequently lead to cosmetic and potentially life-threatening complications. Reconstruction in children presents a unique challenge requiring special surgical techniques often involving several surgeries to compensate for growing and remodeling bones.[2] In adults, craniofacial surgery is usually required after a traumatic skull injury due to combat or accidents, or when

[1]School of Biomedical Engineering, Science and Health Systems, Drexel University, Philadelphia, Pennsylvania.
[2]Department of Genetics and Genomic Sciences, Icahn School of Medicine at Mt. Sinai, New York, New York.
[3]Department of Orthopedic Surgery, Drexel University College of Medicine, Philadelphia, Pennsylvania.
[4]Center for Inflammation, Translational and Clinical Lung Research, Temple University School of Medicine, Philadelphia, Pennsylvania.
[5]Department of Bioengineering, College of Engineering, Temple University, Philadelphia, Pennsylvania.
[6]Department of Natural Sciences and Human Medicine, Michigan State University, East Lansing, Michigan.
[7]Department of Pharmacology and Physiology, Drexel University College of Medicine, Philadelphia, Pennsylvania.

large tumors affect the integrity of craniofacial bones or soft tissues. In 2001, almost 25,000 people in the U.S. needed maxillofacial surgery as a result of trauma.[2]

Bone grafting is the conventional practice in the reconstruction of critical size bone defects, using autologous bone harvested from the patient as the gold standard. However, there are several drawbacks with this method. Grafting introduces a secondary operative site associated with morbidity such as infection and chronic pain.[3,4] If a large graft is needed, it raises a concern for instability and risk of fracture at the donor site and, therefore, limits the amount of available autograft.

An alternative regenerative treatment approach involves the use of biomimetic matrices implanted at the lesion site to encourage bone growth and repair.[5] Within the past 30 years, a variety of different types of biomimetic matrices in place of autologous grafts have been explored. Ideally these would be osteoconductive [promote recruitment of bone (progenitor) cells from the host], osteoinductive (promoting the transformation of bone precursor cells into osteoblasts), and osseointegrative (capable of supporting appropriate host/graft interaction with minimal immune response).[6] These matrices can be composed of either inorganic such as HA,[7–9] organic such as collagen I,[10,11] or synthetic materials such as polymethylmethacrylate (PMMA) or poly (lactic-co-glycolic acid [PLGA]).[12,13]

Electrospinning has emerged as a promising and well-studied platform technology for the fabrication of scaffolds as graft materials. A number of studies have evaluated the potential of electrospun scaffolds for bone tissue engineering and shown that these scaffolding materials are capable of supporting necessary cell adhesion, osteogenic expression, and function.[14–17] Electrospun chitosan (CTS) scaffolds have been shown to specifically aid in osteogenesis and bone tissue engineering applications.[18,19] Previously, we reported that electrospun chitosan/hydroxyapatite microfibrous scaffolds crosslinked with genipin (GP) effectively induce and enhance the osteogenic differentiation and maturation of cultured 7F2 mouse osteoblast-like cells *in vitro*. The individual fibers in the scaffolds were microtextured due to the incorporation of hydroxyapatite nanoparticles. Genipin crosslinking rendered the mechanical properties of the scaffolds similar to those of periosteum.[17]

Successful osseointegration of allografts depends on the presence of periosteum, the functional layer covering bone that contains osteogenic progenitor cells akin to mesenchymal stem cells (MSCs).[20] The periosteum functions as a reservoir of progenitor cells and acts as a bridge to guide cells to the bone defect area. Several groups have focused on recreating the cellular layer of the periosteum.[21–23] As an alternative, MSCs are a renewable cell source that can easily be obtained and differentiated into osteoblasts.[20,24] To date, only a few studies have focused on engineering biomimetic scaffolds that mimic the fibrous layer of the periosteum combined with the cellular layer and that constitute implantable regenerative scaffolds, which can induce/promote bone healing.[25,26] So far, none of these attempts have been implemented clinically.

In this study, we evaluated the ability of our previously described chitosan–hydroxyapatite–genipin scaffolds[17] to support the proliferation of cultured murine mesenchymal stem cells (mMSCs) and their *in vitro* differentiation toward an osteogenic lineage. Using a mouse calvarial defect model, we then assessed the potential of our scaffolds to integrate with the host tissue *in vivo*. Our results show that these scaffolds can provide an appropriate environment to initiate MSC differentiation, while supporting the formation of multilayered tissue-like formation *in vitro*. Moreover, the mineralized scaffolds promote *in vivo* osseointegration with the host tissue, as demonstrated by enhanced defect closure and new tissue formation around the periphery of the lesions.

Materials and Methods

Materials

Medium molecular weight CTS (75–85% deacetylated), trifluoroacetic acid (TFA, ≥98%), HA (reagent grade, <200 nm nanoparticles), 1,1,1,3,3,3-hexafluoro-2-propanol (HFP), ascorbate-2-phosphate, β-glycerosphosphate, ferric chloride, Beibrich's Scarlet, Acid Fuchin, phosphomolybolic acid, and phosphotungstic acid were purchased from Sigma-Aldrich Co. Ltd. (St. Louis, MO). Hematoxylin, Eosin Y, 37% formaldehyde, hydrochloric acid (HCl), Aniline Blue, and Permount were purchased from Fisher Scientific (Kalamazoo, MI). Picric acid was from EMS (Hatfield, PA). Decalcifying solution (Cal-Ex) was purchased from Fisher Scientific. GP (≥98% pure) was purchased from Wako Pure Chemical Industries Ltd. (Osaka, Japan). The alamarBlue™ colorimetric assay kit was from AbD Serotec (Raleigh, NC). The alkaline phosphatase colorimetric assay was purchased from Abcam (Cambridge, MA). Xylene was purchased from VWR Laboratories (West Chester, PA). Dexamethasone was from Alfa Aesar (Ward Hill, MA).

Murine mesenchymal stem cells (mMSCs) were kindly provided by Dr. Darwin Prockop (the University of Texas A&M, Institute of Regenerative Medicine). CD-1 strain female mice (~30 g) were purchased from The Jackson Laboratory (Bar Harbor, ME). All surgical supplies were purchased from PennVet (Lancaster, PA). Trephines (2.1 mm diameter) were purchased from Fine Science Tools (Foster City, CA).

Fabrication of electrospun and modified chitosan scaffolds

CTS and CTS-HA-containing scaffolds were electrospun as previously described.[17] Briefly, 7% (w/v) CTS was dissolved in TFA and electrospun at 1.0 mL/h, 15 kV, and a 15 cm working distance. HA-containing scaffolds were generated by admixing 1.0% HA nanoparticles (w/v) to the CTS solution before spinning. All solutions were stirred at room temperature for at least 5 days. The scaffolds were first stabilized (waterproofed) by soaking them for 20 min in 0.5% sodium hydroxide (NaOH) dissolved in 100% ethanol, followed by five 30 s washes with 1× phosphate buffer solution (PBS) to remove any trace amounts of ethanol.[27] The stabilized scaffolds were then crosslinked in 0.1% (w/v) GP dissolved in 1× PBS for 24 h. Resulting scaffolds were either GP-crosslinked chitosan scaffolds (CTS-GP) or genipin-crosslinked hydroxyapatite-containing chitosan scaffolds (CTS-HA-GP).

Maintenance and multipotency of mMSC in culture

Cell culture. Murine MSC (mMSC) were maintained in Iscove's modified Dulbecco's medium (IMDM) containing

1 g/L glucose and supplemented with 10% fetal bovine serum + 10% horse serum, 2 mM L-glutamine and 2% antibiotic–antimitotic (ABAM). Cells were placed in T75-cell culture flasks in an incubator set to 37°C and 5% carbon dioxide. The medium was changed every third day. The cells were passaged at a ratio of 1:3 three times by trypsinization before seeding on the scaffolds. Multipotency of mMSCs was ascertained by culturing the cells for 3 weeks in either an osteogenic medium (OGM) containing DMEM (4.5 g/L glucose) containing 100 nM dexamethasone, 500 μM ascorbate-2-phosphate, and 10 mM β-glycerophosphate, and staining with Alizarin Red S, or in a serum-free chondrogenic medium containing 1% 100× ITS + 3 (insulin, transferrin, and selenium), 1.25 mg/mL bovine serum albumin (BSA), 100 nM dexamethasone, 2000 μM ascorbate-2-phosphate, 1 mM sodium pyruvate, and 10 ng/mL transforming growth factor-β3 (TGFβ3), and staining with Alcian Blue (Supplementary Fig. S1; Supplementary Data are available online at www.liebertpub.com/tea).[28]

Cell seeding. Circular scaffolds with a diameter of 10.3 mm, cut from either the CTS-HA-GP (1.0% HA) or CTS-GP electrospun sheets, were placed in 24-well plates, secured with a Viton O-ring,[29] stabilized, and crosslinked with 0.1% GP, as described above. The samples were sterilized using 10% ABAM overnight and then subsequently washed three times with DI water and left overnight in complete IMDM. The next morning, the medium was aspirated and the scaffolds seeded by carefully pipetting 50 μL of the mMSC suspension containing 500,000 cells onto the center of the scaffold. The cell-seeded scaffolds were then placed into an incubator for 1 h. After this time period, 450 μL of complete IMDM or OGM was added to each well, as per the specific experimental conditions. The cells were cultured for up to 21 days, during which time the medium was changed every third day. Cells were also cultured in a similar manner on tissue culture polystyrene (TCP) as a negative control.

Cell morphology. The morphology of the cells was visualized by fluorescent microscopy. All cells were cultured on 10 mm diameter circular scaffolds and TCP controls, as described above. The cells were fixed at days 7, 14, and 21 and stained with DAPI/phalloidin staining to visualize mMSC morphology on the various substrates, as previously described.[30] Briefly, scaffolds were fixed in 10% formalin at the above-mentioned time points for 20 min followed by subsequent washing with distilled deionized (DDI) water and 60 mM glycine. The fixed cells were permeabilized with 0.5% Triton-X 100 for 20 min and then washed three times for 10 min each in immunofluorescent wash containing 130 mM NaCl, 7 mM Na_2HPO_4, 3.5 mM $Na_2H_2PO_4$, 7.7 mM NaN_3, 0.1% BSA, 0.2% Triton-X 100, and 0.05% Tween-20 in DI water, which greatly reduced scaffold autofluorescence. The samples were then incubated for 15 min with a 1:1000 dilution of FITC-phalloidin, washed three times, and mounted in Vectashield® medium containing DAPI (from Vector Labs, Burlingame, CA). All images were obtained using a Z1 Observer light microscope (Zeiss, Thornwood, NY) at 10× magnification. All analyses were performed using the Axiovision (Zeiss) software.

Cell viability and proliferation. Cell viability and proliferation were continually monitored over a 21 day period using the alamarBlue™ assay, as previously described.[31] In brief, mMSCs were seeded in 24-well plates onto TCP as well as onto circular CTS-GP and CTS-HA-GP scaffolds at a density of 500,000 cells per well, as described above. On days 0, 3, 7, 14, and 21, AB was added at 10% (v/v) in triplicate wells. The plates were then returned to the incubator for 3 h. For zero control, AB was also either added to wells containing only medium or scaffolds and media. After 3 h, 200 μL aliquots of the supernatant were pipetted in triplicate into 96-well plates and the AB fluorescence was read in a Synergy 4 microplate reader (Biotek, Winooski, VT) at an excitation wavelength of 545 nm and an emission wavelength of 590 nm. The data were analyzed using the Gen5 software (Biotek) and samples were normalized to their respective zero controls. The cells were refed with fresh medium and placed in the incubator to be analyzed at the next time point.

Alkaline phosphatase activity. To assess the osteogenic potential of our scaffolds we seeded mMSCs, as above, in IMDM or OGM on TCP, CTS-GP, and CTS-HA-GP scaffolds and measured the activity of alkaline phosphatase (ALP), which is an established early marker for MSC differentiation toward the osteoblast phenotype.[32] ALP activity was measured colorimetrically on days 0, 7, 14, and 21 using a commercial kit (ab83369; Abcam). At each time point, three cell-seeded scaffolds were homogenized in a glass tube homogenizer containing 300 μL of lysis buffer (kit component). The supernatant was collected and centrifuged at 350 *g* for 3 min to remove all insoluble debris. Thirty-microliter aliquots of the resultant samples were added to a 96-well plate followed by 50 μL of assay buffer and 50 μL of *para*-nitrophenylphosphate (pNPP) solution. Following incubation for 1 h at room temperature, 20 μL of stop buffer was added to the samples and the absorbance was read in the microplate reader at 420 nm, as previously described.[17] To measure the ALP activity of control cells growing on TCP, the wells were rinsed with 300 μL of 1× PBS, followed by the addition of 300 μL 1× lysis buffer for 10 min. After that, the supernatant was collected and cell remnants were scraped with a cell scraper for manual lysis. The ALP activity was analyzed, as above. Results are presented as fold increase compared with the cells cultured on TCP.

Osseointegrative capacity of the scaffolds

Cell culture for *in vivo* implantation. CTS-GP and CTS-HA-GP scaffolds were cut into 10 mm circular scaffolds, fitted into 24-well plates and held in place using Viton O-rings.[33] The scaffolds were sterilized in 10% ABAM overnight and subsequently washed three times with DI water and incubated with IMDM medium overnight.

MSCs were cultured in complete IMDM in conventional T-75 cell culture flasks, split at a ratio of 1:3 and expanded for two passages. Undifferentiated (naive) stem cells were seeded onto the various scaffolds 3 days before implantation at a seeding density of 500,000 cells per scaffold. Immediately before implantation, 2.5 mm circular samples were cut aseptically using a punch biopsy from the various

scaffolds (CTS-GP and CTS-HA-GP scaffolds with and without cells) placed into a Petri dish containing 1× PBS with calcium and magnesium and transported aseptically into the surgery room.

Animal studies. CD1 female mice ($n=48$) weighing ~30 g (4–6 weeks) were obtained from Jackson Laboratories (Bar Harbor, ME). Mice were housed in cages with *ad libitum* access to food and water and maintained on a 12-h light–12-h dark schedule. A maximum of five mice were housed in a single cage. Cages were cleaned daily and all mice were allowed to acclimate for 1 week after arrival to the laboratory before any surgical procedures were performed.

All surgical procedures and postoperative care were in accordance with an Institutional Animal Care and Use Committee (IACUC)-approved protocol. In brief, animals were anesthetized with isofluorane (3 L/min) (E-Z Systems, Palmer, PA) for 15 min and placed into a stereotaxic frame (David Kopf Instruments, Tujunga, CA). Once secured in the stereotaxic frame, the animals were maintained on 1.5–2.0 L/min isofluorane delivered through a surgical mask. Ketoprofen (5 mg/kg) was administered subcutaneously for prophylactic treatment for pain and inflammation. An incision was made along the sagittal axis and the skin was deflected laterally to expose the underlying cranium. A stereotaxic microdrill (Foredom, Bethel, CT) fitted with a microtrephine (2.3 mm external diameter; Fine Science Tools) was used to remove two circular sections of bone from each side of the skull. One of these lesions was covered with one of the scaffolds (cell-free or cell-seeded, as mentioned above), while the contralateral lesion was left untreated as a control to ensure that the wound was, in fact, critical size. A small dab of Vetbond surgical glue (3M, St. Paul, MN) was applied to the tip of a stainless steel insect pin (size 00) and used to fasten the underside of the apices of the scaffold to the underlying bone and prevent shifting following surgery. Animals were given subcutaneous ketoprofen (2 mg/kg) injections 12 and 24 h postsurgery for pain management. Mice were sacrificed at 1, 2, and 3 months and calvaria were studied for regeneration. Of the 48 animals, 3 mice died during surgery and 2 postsurgery.

Euthanasia and harvesting of tissue. Animals were sacrificed by induction with isofluorane followed by an overdose of intraperitoneally administered Beuthanasia (Merck Animal Health, Summit, NJ). The head was then detached with sheers and the skin was fully removed from the skull. Harvested skulls were placed in 10% formalin in 4°C overnight for fixation and then stored in 1× PBS until further processing and analysis.

MicroCT imaging and defect area measurements. New bone formation and the density of new tissue formed postsurgery were assessed by microCT, using a Viva40 μCT-50 scanner (Scanco Medical, Wayne, PA) housed at the University of Pennsylvania School of Veterinary Medicine, Department of Animal Biology (Philadelphia, PA). The scanner was run with an X-ray energy/intensity of 70 kVp, 114 μA and 8 W; a medium resolution; a scout view reading from 0 to 145 mm and angle of 90°; an FOV diameter of 38.9 mm; a voxel size of 38 μm; and an integration time of 200 ms. The number of slices was 211/8.02 mm, equivalent to 38 μm/slice. Wound morphology and area measurements were carried out on reconstructed images using the Axiovision (Zeiss) and ImageJ Imaging Softwares.[34,35] For each time point, the area of the treated defects was normalized to the area of the untreated contralateral control defects and is presented as a percentage of wound closure. Zero time control defects were created by drilling standard defects into three animals, followed by immediate euthanasia and averaging the circular area of the defects (at time 0).

Hematoxylin/eosin and Masson's Trichrome staining for bone formation. Following acquisition of the microCT images, fixed samples were decalcified in Cal-Ex decalcifying solution (Fisher Scientific) until the skull bone lost its rigid texture and became softer and more pliable (~10 days). After decalcification, the calvaria was excised from the rest of the skull, serially dehydrated in EtOH (75%, 85%, 95%, and 100% twice) and xylene (50:50 ethanol: xylene, followed by 100% xylene twice) for 15 min each, and finally embedded in paraffin. Paraffin-embedded samples were frozen at −20°C overnight and then sectioned transversely into 5 μm slices using a Leica R2255 microtome (Buffalo Grove, IL). Slices were placed in a warm water bath and then mounted onto poly-L-lysine-coated slides and allowed to dry overnight.

Routine Hematoxylin and Eosin (H&E) staining was used to assess the integration of the scaffolds with the host tissue. Briefly, tissue sections were rehydrated through a serial xylene/ethanol/water rehydration procedure then stained with H&E following standard procedures (IHC World, Woodstock, MD). Conventional Masson's Trichrome staining was used to visualize the organization of the newly formed tissue around the injury site, especially the presence of collagen. Samples from both stains were mounted with Permount and viewed under bright light illumination in a Leica DMRX microscope.

Statistical analysis

All cell culture studies were performed three times independently in triplicate unless stated otherwise. Animal studies were performed according to an IACUC-approved protocol with four animals per group, deemed statistically significant by power calculations using the GPower software and a pilot study. Where indicated, all data are presented as means ± standard deviation. A two way-ANOVA analysis was used with Tukey *post hoc* analysis performed to record power values of $p>0.05$ (*) or $p>0.01$ (**).

Results

CTS-HA-GP scaffolds support proliferation and osteogenic differentiation potential of cultured mMSC

A scanning electron microscopy image of typical electrospun nanofibers crosslinked with genipin is shown in Figure 1. Details of the morphology of HA-containing mineralized, genipin-crosslinked fibers are shown at higher magnification (insert). The nano-sized protrusions (~25 nm in diameter, see arrows) on the fibers represent HA nanoparticles studded throughout the fibrous network, as previously demonstrated using several independent techniques, such as X-ray diffraction, Fourier transform infrared spectroscopy and energy

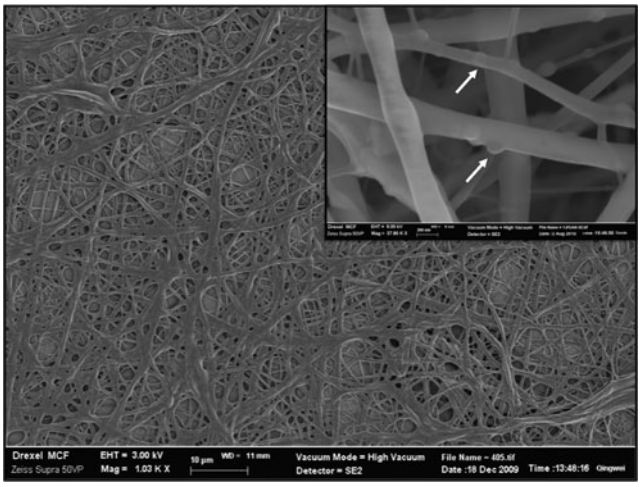

FIG. 1. Morphology of electrospun CTS-HA-GP scaffolds. Scanning electron micrographs of electrospun mineralized scaffolds (original magnification: 1000×) indicate a network of randomly oriented, beadless fibers. The *insert*, taken at higher magnification (5000×), shows the presence of hydroxyapatite (HA) nanoparticles studding the surface of the electrospun fibers (*white arrows*). Scale bars are 100 µm (*main figure*) and 200 nm (*insert*), respectively. CTS, chitosan; GP, genipin.

dispersive X-ray spectroscopy.[17] The average fiber diameter of both the crosslinked CTS-GP and CTS-HA-GP scaffolds, was 334.7 ± 119.1 nm ($n = 10$ independent samples, analyzing ~50 fibers/sample), similar to the values reported previously.[17] The Young's modulus of composite scaffolds was 142 ± 13 MPa, also as previously reported.[17]

To investigate the capacity of the various scaffolds to support MSC proliferation and potential osteogenic differentiation, mMSCs were seeded onto nonmineralized (CTS-GP) and mineralized (CTS-HA-GP) scaffolds and assessed for cell morphology, metabolic, and ALP activity. Adhesion, spreading, and proliferation of mMSCs on both scaffolds were visualized by fluorescence microscopy, using DAPI/phalloidin staining of nuclei and cytoskeleton, respectively. The scaffolds were placed in 24-well plates, seeded with 500,000 cells per well, and imaged after 1 and 3 weeks of culture. The cells formed confluent monolayers essentially, completely covering the scaffolds after 1 week, and maintained confluence for the duration of our study irrespective of the scaffold type (Fig. 2A–D). A 3D rendering of DAPI-stained fluorescent nuclei of the cells seeded onto CTS-HA-GP scaffolds showed a three-fold increase ($p > 0.05$) in the thickness of the cell layer at 2 weeks when compared to 1 week (Fig. 2E, F) from 8 to 24 µm. Similar results were observed on CTS-GP scaffolds (not shown).

AB is widely used to assess the metabolic activity of cultured cells. This metabolic activity can serve to indirectly suggest whether cells are in a state of proliferation or differentiation.[36] As seen in Figure 3A, AB fluorescence readings, that is, the metabolic activity of mMSCs, increased throughout the first week and then decreased by day 10 on all scaffold and medium types. After 2 weeks, the metabolic activity plateaued at a level below that of freshly seeded scaffolds. In conventional viability studies, such a decrease in the readout of indicators of metabolic activity is often equated with a decrease in cell numbers.[37] However, because in our case the cell layers maintained confluence on the scaffolds (Fig. 2A–D), we attribute the decrease in AB fluorescence after day 10 followed by an invariant plateau at the later time points to a shift from proliferation to enhanced (osteogenic) differentiation, and with that a lower metabolic activity of the cells, rather than cell death.

To assess the potential of our scaffolds to induce osteogenic differentiation of cultured mMSCs, we quantified the enzymatic activity of ALP over time. The data were normalized to the ALP activity of cells cultured in parallel on TCP. As seen in Figure 3B, at both days 7 and 14, all conditions show a slight increase when compared to TCP, except CTS-GP without cells at day 7, which is lower than TCP. Interestingly, the combination of OGM and HA, at these stages, did not significantly enhance osteogenic differentiation. By contrast, on day 21, a

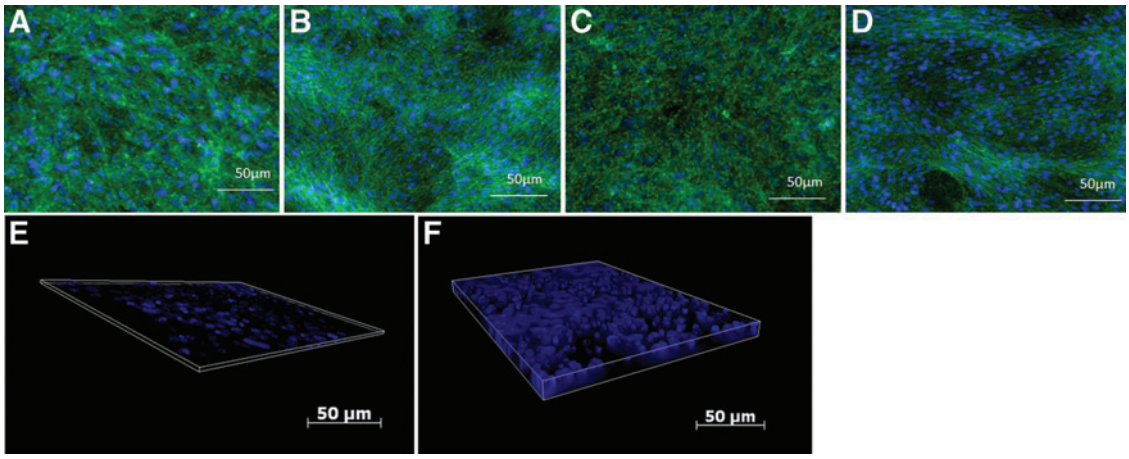

FIG. 2. Morphology of murine mesenchymal stem cells (mMSCs) seeded onto chitosan (CTS) scaffolds. **(A–D)** Cells cultured on CTS-GP scaffolds at 1 week **(A)** and 3 weeks **(C)** and CTS-HA-GP scaffolds at 1 week **(B)** and 3 weeks **(D)** were fixed and stained with DAPI (nuclei, *blue*) and Phalloidin (F-actin, *green*). The cultures quickly reached and then maintained confluence throughout the study. **(E, F)** Three-dimensional renderings of the scaffolds demonstrated a three-fold increase ($p > 0.05$) in thickness of the cellular layer between 1 week **(E)** at 8 µm and 2 weeks **(F)** at 24 µm. Scale bars for all *panels* = 50 µm, original magnification for all images: 10×. Color images available online at www.liebertpub.com/tea

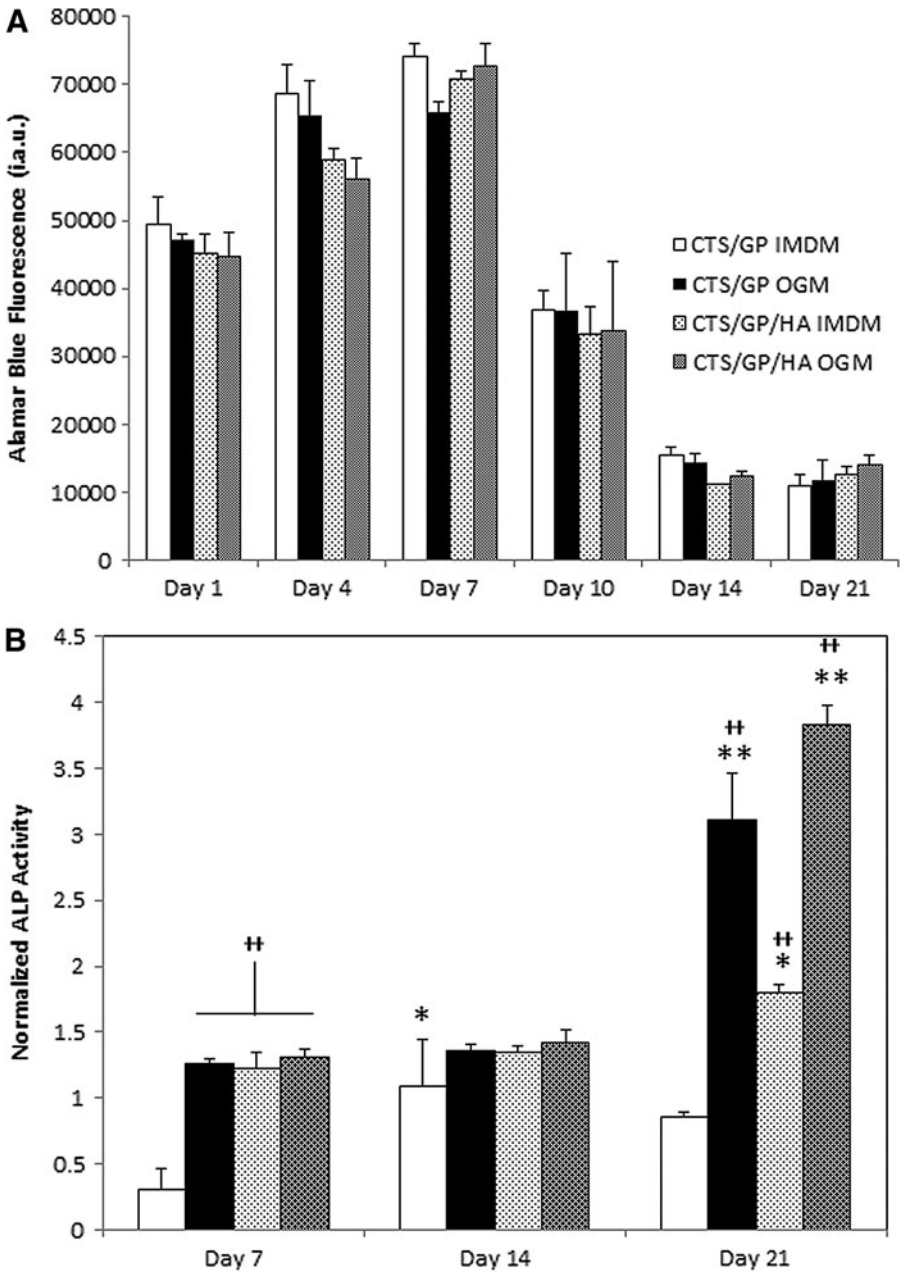

FIG. 3. The alamarBlue™ fluorescence and alkaline phosphatase (ALP) activity of mMSCs seeded onto the various scaffolds. Murine MSCs were seeded onto the various scaffolds in either maintenance medium (Iscove's modified Dulbecco's medium) or osteogenic medium (OGM). AB fluorescence (for metabolic activity) and ALP activity (for osteogenic differentiation) were measured at the times indicated (for details see Materials and Methods section). All data are presented as means ± standard deviations. Sample size was $n = 3$ (in triplicate) with $^{*}p < 0.05$ and $^{**}p < 0.01$ compared with the previous time points of the same group and $^{++}p < 0.01$ compared with the CTS-GP control group at the same time point. **(A)** Continual measurement of alamarBlue™ fluorescence revealed that by day 10 the metabolic activity of mMSCs decreased on all scaffolds, and plateaued until day 21 (data are expressed as arbitrary fluorescence units). **(B)** ALP activity normalized to mMSCs cultured in parallel on tissue culture polystyrene (TCP), increased in the presence of HA and OGM when compared with CTS-GP cultures alone.

significant increase of 3.1 ± 0.4- and 3.8 ± 0.2-fold in ALP activity was seen in cells cultured in OGM on CTS-GP and CTS-HA-GP scaffolds, respectively. A significant, albeit somewhat lower (1.8 ± 0.1-fold) increase was also observed in cells on CTS-HA-GP scaffolds in maintenance medium. By contrast, ALP activity of cells cultured on CTS-GP scaffolds in maintenance medium was indistinguishable from that of cells cultured on TCP. Taken together, we conclude that cells on CTS-GP scaffolds are more likely becoming quiescent, whereas cells on CTS-HA-GP are undergoing a shift toward the osteogenic phenotype.

Osseointegrative capacity of CTS-HA-GP scaffolds

To test the osseointegrative capacity of our scaffolds *in vivo*, that is, the ability to allow the host tissue to incorporate into the constructs, we implanted CTS-GP or CTS-HA-GP scaffolds, with or without naive mMSCs preseeding, into critical size calvarial defects, as detailed in the Materials and Methods section. Samples were harvested after 1, 2, and 3 months and analyzed histologically and by microCT.

Representative microCT images for all scaffolds and conditions are shown in Figure 4 and Supplementary Figure S2. One month after injury, very little mineralized tissue formation was discernible, irrespective of whether the lesions were treated with mineralized or nonmineralized scaffolds, and whether the scaffolds had been preseeded, seeded with mMSCs, or not. Quantification of the cumulative results indicated a trend, in which mineralized scaffolds with or without cell seeding induced more wound closure than the nonmineralized scaffolds, albeit at a low scale. After 2 months, there was a significant (~25%) increase in *de novo* bone formation for lesions covered with mineralized, MSC-

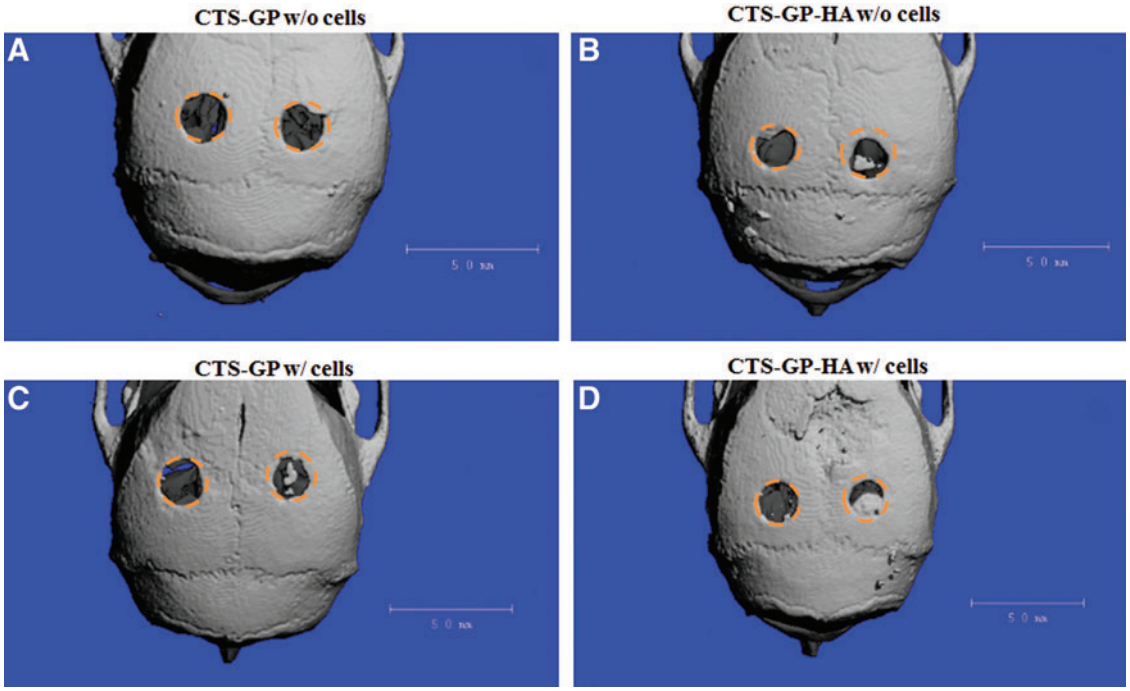

FIG. 4. Reconstructed microCT images of calvarial defect treatments. Formation of new mineralized tissue at 3 months. The size and location of the original lesions are depicted by the *orange circular* regions of interest. Representative μCT images are shown. **(A)** CTS-GP scaffolds without cells; **(B)**: CTS-GP-HA scaffolds without cells; **(C)**: CTS-GP scaffolds with cells; **(D)**: CTS-GP-HA scaffolds with cells. Scale bar = 5 mm. Color images available online at www.liebertpub.com/tea

seeded CTS-HA-GP scaffolds, whereas lesions treated with cell-free nonmineralized scaffolds showed a smaller, but significant ~10% decrease in the wound area. By contrast, wounds treated with nonmineralized CTS-GP scaffolds, with and without cells, still showed minimal bone formation. By 3 months, ca. 30% wound closure was observed in lesions treated with cell-seeded nonmineralized CTS-GP scaffolds, whereas in the absence of cells, novo tissue formation induced by the nonmineralized scaffolds still remained minimal (Fig. 4A, B, respectively). Importantly, at this time point, lesions treated with mineralized CTS-HA-GP scaffolds, without and with cells, showed a 35% and 45% decrease in the wound area, respectively, when compared to untreated control (Figs. 4C, D, and 5).

Taken together, these results suggest that 3 months after injury, wound healing in lesions treated with nonmineralized scaffolds requires additional preseeding with mMSCs, whereas in the case of mineralized scaffolds, the CTS-HA-GP scaffolds alone, even without preseeding MSCs, are essentially equally effective in promoting osseointegration and new bone growth.

To histologically assess osseointegration, decalcified skulls were stained with both H&E and Masson's Trichrome stain (MTS) and evaluated histologically. As seen in Figure 6A and B, after 3 months the nontreated wounds were lined by a thin fibrous layer, mostly comprised of collagen (which is characterized by blue color in MTS, see especially insert in Figure 6B), indicating the formation of fibrous scar tissue. In contrast, in animals implanted with CTS-HA-GP scaffolds for 3 months, new tissue formation could be seen along the host/scaffold interface (Fig. 6C, D). This regenerating tissue contained both collagen fibers (blue) and

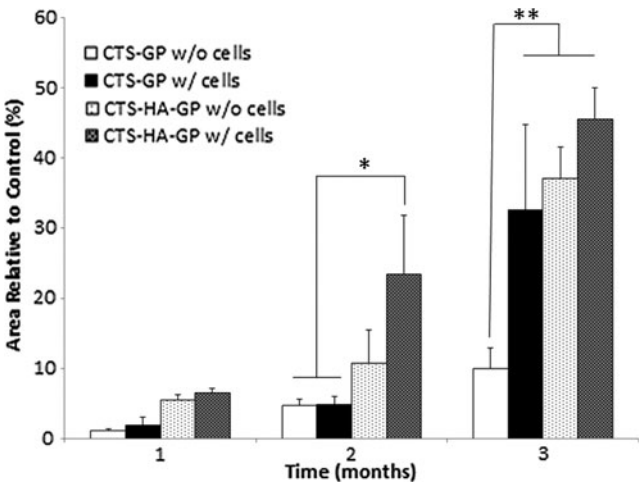

FIG. 5. Bone regeneration in critical size calvarial defects. The percentage (%) of defect closure in the presence of the scaffolds was normalized to the size of the contralateral nontreated control defects in each sample at every time point. No or minimal healing was observed in untreated defects at all times. Nonmineralized scaffolds were effective after 3 months, but only when preseeded with mMSCs. Most pronounced healing over time was observed in lesions treated with scaffolds preseeded with mMSCs. However, at 3 months there was no statistically significant difference in the percentage of wound closure in lesions treated with mineralized scaffold without or with cells. For details see text. Data are presented as means ± standard deviations. The sample size (number of individual mice) was $n = 4$ for all measurements, with $^{*}p < 0.05$ and $^{**}p < 0.01$ compared with nonmineralized scaffolds.

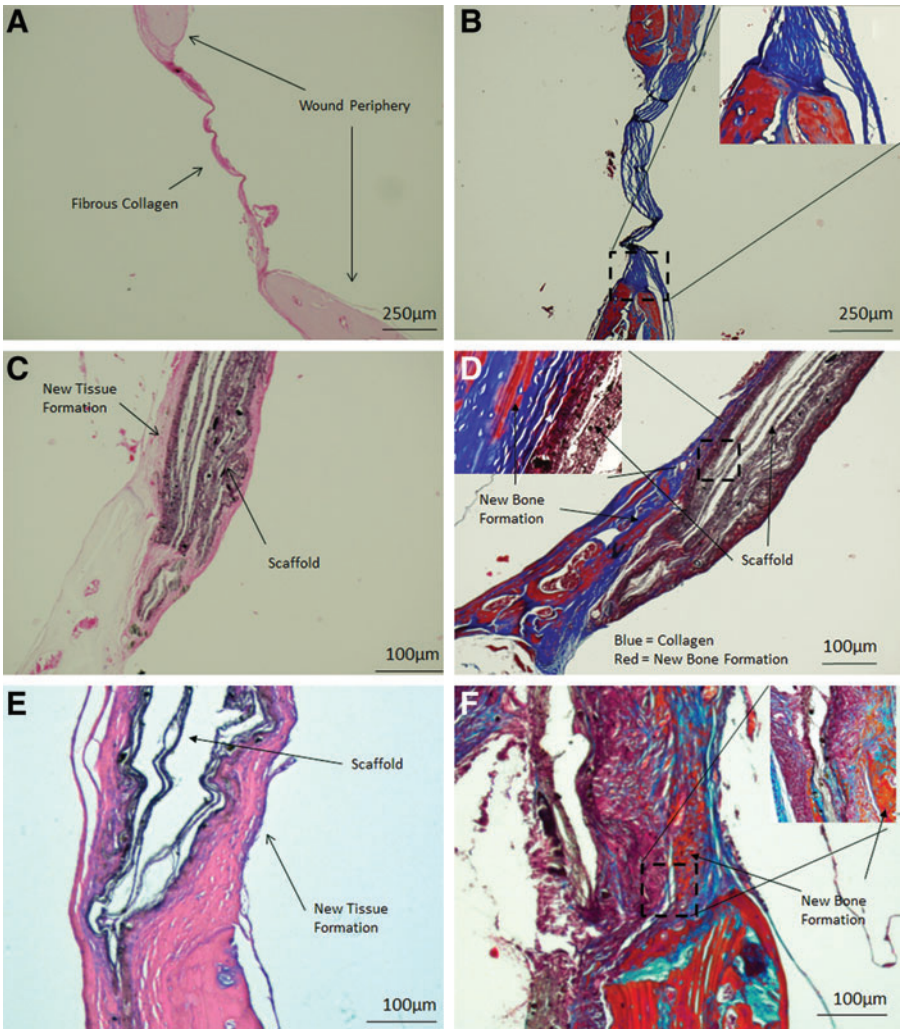

FIG. 6. Histology of healing of critical size calvarial defects 3 months after injury. Nontreated defects show no or minimal wound healing and coverage of the lesion with a thin fibrous layer that is comprised of collagen. **(A)** Hematoxylin and Eosin (H&E) staining, **(B)**: Masson's Trichrome stain (MTS), original magnification of **(A, B)** is 40×. H&E **(C)** and Masson's Trichrome **(D)** staining of defects treated with CTS-HA-GP scaffolds without mMSCs show new bone formation (*red*), collagen deposition (*blue*), and significant scaffold interaction. Original magnification 40×, *inserts* are 100×. H&E **(E)** and Masson's Trichrome **(F)** staining of defects treated with CTS-HA-GP scaffolds pressed with mMSCs indicates very similar results to those scaffolds without cells, but does appear to have enhanced tissue growth and new bone formation along the periphery of the scaffold (brown). Higher magnification of a defect treated with CTS-HA-GP scaffolds seeded with mMSCs reveals endochondral-like tissue formation along the host–scaffold interface **(F)**. Original magnification 40×, *inserts* are 100×. Magnification for **(C–F)** are 100×. For details, see text. Scale bars: **(A, B)**: 250 μm; **(C–F)**: 100 μm. Color images available online at www.liebertpub.com/tea

new bone (red) as well as remnants of the genipin-crosslinked scaffold material, indicating the degradation of the scaffold material and its replacement with new bone tissue (Fig. 6D). The insert in Figure 6D depicts, at higher magnification, abundant presence of collagen (blue) and formation of new bone (red) along the scaffold, especially along the outer surface of the wound periphery. The composite CTS-HA-GP scaffolds on its own induced significant new bone formation and collagen deposition. Osseointegration was further enhanced by treating the lesions with scaffolds preseeded with mMSCs (Fig. 6E, F), as inferred from the greater abundance of collagen (blue) and bone (red) that, for example, in Figure 6D. This latter observation also is in line with the analysis of the microCT data (Fig. 5).

Discussion

Optimized biomimetic scaffolds for bone tissue engineering will provide physical and chemical cues capable of supporting tissue-specific differentiation of progenitor cells *in vitro* (osteoinduction) and ingrowth of/integration with the surrounding host tissue *in vivo* (osteoconduction). The major finding of this study is that electrospun genipin-crosslinked chitosan scaffolds, mimic certain features of the mineralized fibrillar nanostructure of native bone tissue, initiate regeneration and tissue interaction, and support osseointegration in a murine model of critical size calvarial defects *in vivo*. More specifically, our mineralized scaffolds efficiently facilitate mMSCs growth/proliferation and osteogenic differentiation *in vitro* (Figs. 2 and 3) and promote the repair of critical size cranial defects and the integration of the scaffolds with the surrounding host tissue *in vivo* (Figs. 4–6). Most importantly, our mineralized chitosan scaffolds, crosslinked with genipin and containing HA nanoparticles (Fig. 1), can trigger regeneration of critical-size calvarial defects in a mouse model without the need for preseeding the scaffolds with MSCs (Fig. 5). This observation may be significant for translating our findings into the clinical realm, enabling the production of cell-free bioactive mineralized scaffolds with prolonged shelf life.

The ability of HA in composite materials to stimulate osteogenesis has been shown in several studies.[38–40] For example, Liu *et al.* demonstrated that the deposition of HA from simulated body fluid onto nanofibrous/macroporous gelatin scaffolds enhanced their mechanical properties and also significantly increased the expression of osteogenic markers in murine MC3T3-E1 osteoblasts cultured on/in these scaffolds.[38]

A variety of manufacturing techniques, such as thermally induced phase separation or electrospinning[38,39] can be used

to directly incorporate HA into the polymer matrix of composite scaffolds, whereas surface coating of electrospun matrices with HA can be achieved by electrodeposition.[39] To the best of our knowledge, except of our own previous publication,[17] there are no other reports on the direct incorporation of HA into fibers electrospun out of pure chitosan (in the absence of additives, such as poly[ethylene oxide] [PEO][41,42] and crosslinked with genipin).

Composite electrospun scaffolds containing chitosan and other biomaterials, such as collagen and PLGA, have previously been shown to promote MSC attachment/proliferation and osteogenic differentiation *in vitro*.[43,44] To the best of our knowledge, no one has yet studied these effects using pure electrospun CTS-GP or CTS-HA-GP scaffolds. The metabolic activity and/or proliferation of cells cultured on bioactive scaffolds *in vitro* are frequently assessed using the alamarBlue™ assay.[37,45] The sizeable decrease in AB fluorescence (mMSC metabolic activity) after 10 days in culture, as seen in Figure 3A, could be due to either a decrease in the number of viable cells, or, alternatively, to the enhancement of their quiescence/differentiation.[36,45,46] As seen in Figure 2, the cell numbers did not decrease over time; on the contrary, the cells maintained and expanded their multilayered configuration and continued to cover the scaffold surface over the remaining experimental duration (3 weeks). Taken together these data suggest that the observed decrease in AB fluorescence after 10 days in culture might indicate the inception of cell differentiation, rather than a loss of cell numbers/viability, or entry into cellular quiescence.

In support of the notion of enhanced differentiation, mMSC, ALP activity was significantly increased at day 21 (Fig. 3), which, in conjunction with our AB data, we interpret to indicate that the mMSCs seeded onto CTS-HA-GP scaffolds are differentiating toward an osteogenic phenotype, even in the absence of an OGM. Previously, we showed parallel induction of ALP and other more specific markers of osteogenic differentiation markers, such as osteonectin and osteopontin in 7F2 osteoblasts that were cultured on our composite scaffolds.[17] In this study, ALP served as a surrogate marker for osteogenic differentiation of mMSCs, in line with several published reports, in which ALP has been used as a common marker for osteogenic induction[47,48] and osteogenic differentiation of MSCs.[49,50]

As seen in Figure 3B, ALP was always higher when the cells were cultured on the mineralized scaffolds. Furthermore, ALP activity of the cells on the scaffolds, both nonmineralized and mineralized, was further enhanced twofold to threefold in the presence of an OGM, indicating an additive effect between the chemical cues in the differentiation medium and the osteogenic properties of the electrospun scaffolds. These three independent observations (cell visualization, AB fluorescence, and enhanced ALP activity) support the notion that the addition of HA can aid in promoting osteogenic differentiation of cultured mMSCs.

The enhanced osteogenic capacity of HA-containing scaffolds may, in part, also be due to their unique submicron topography. Indeed, topographical properties of micro- and nanoscale grooves and pits as well as the incorporation of nanoparticles of hydroxyapatite, zinc, and other naturally occurring inorganics in the body lead to enhanced spreading and production of cultured human osteoblasts.[51] Accordingly, our data, both *in vitro* and *in vivo,* suggest that the presence of HA in the scaffolds promoted osteogenic differentiation and osseointegration (Figs. 4–6).

For our *in vivo* studies we used both cell-free scaffolds and scaffolds seeded with naive mMSCs. Implanting undifferentiated MSCs may have certain advantages to seeding predifferentiated MSCs. Naive MSCs exhibit bystander cell effects, that is, they release factors that promote cell migration, proliferation, and differentiation of other cell types, leading, for example, to enhanced chondrocyte proliferation *in vitro,*[52] or enhanced cartilage formation in the presence of undifferentiated MSCs *in vivo*.[53] Furthermore, naive MSC exhibit immunosuppressive properties[54,55] and reduce unwanted side effects of immune responses and rejection as inferred from the reportedly beneficial adjuvant effects of MSCs in organ transplantation.[56]

The microCT data (Figs. 4 and 5) indicate that nonmineralized CTS-GP scaffolds induce only moderate defect healing, that is, $\sim$10% area closure compared with control defects over a 3 month period. However, the incorporation of mMSCs and/or HA significantly enhanced the tissue regenerative properties of the CTS-GP scaffolds, as indicated by 35% gap closure, when implanting mMSCs-seeded, nonmineralized scaffolds and 40% and 45% when the scaffolds contained HA alone or in combination with mMSCs (Figs. 4 and 5 and see also Supplementary Fig. S2).

Given the significant enhancement of wound closure by MSC-seeded scaffolds, we attempted in preliminary studies to localize seeded GFP-expressing MSCs in the wound using an *in vivo* imaging system. At the earliest time point investigated, (1 months postseeding) we were unable to trace MSCs in the wound area. Our failure to visualize labeled MSCs 1 month after implantation is in line with the reported short-term ($<$14 days) survival of these cells.[57] Nevertheless, it is remarkable that in spite of their short survival at the site of lesion, transplanted MSCs are capable to enhance the beneficial effects of the nonmineralized chitosan scaffolds over a period of 3 months. The time course and duration of MSCs survival postimplantation and the mechanisms, how these cells enhance wound closure, are currently under investigation in our laboratory.

Semiquantitative analysis of the microCT data in terms of percentage reduction in the area of the lesion indicates significant formation of new, mineralized bone after 3 months (up to 45%) under optimized conditions using mineralized scaffolds (Figs. 4 and 5 and Supplementary Fig S2). Our results are in line with other studies indicating the regenerative capacity of biomimetic electrospun scaffolds.[58–60] For example, Zhu *et al.*[58] electrospun core-shell nanofibrous scaffolds from polyethyleneglycol/polycaprolactone (PCL) and incorporated human recombinant BMP-2 for controlled release at the site of a critical size cranial defect in rabbits. After 3 months the extent of wound healing induced by the optimized drug-laden scaffolds was $\sim$35%. Similarly, Schofer *et al.*[61] [using a rat calvarial critical size defect model reported results very similar to ours, namely that electrospun scaffolds made of poly((L)-lactic acid), PLLA] and incorporating BMP-2 induced some 45% wound closure in 12 weeks, whereas the PLLA scaffolds by themselves were essentially ineffective. Finally, electrospun scaffolds made of PCL/poly(methylmethacrylate) microfibers enhanced the healing of cranial defects to a degree that was similar to the one seen with our scaffolds.[61]

While the rate and degree of wound closure obtained in our study are similar to the values reported in the literature, the main difference of our approach to most other ones is that, in our case, the mineralized scaffolds themselves, in the absence of exogenous growth factors, are bioactive. This is certainly an advantage in terms of cost efficiency and simplifying the manufacturing process, and with that of potentially translating our findings into a clinical setting. As another advantage, we note that the mechanical properties (Youngs/compressive modulus) of our mineralized scaffolds[17] exceed those of electrospun scaffolds used by others[41,61] for repairing calvarial defects by approximately two orders of magnitude, that is, ca. 140 MPa versus 1–4 MPa.

Histological analysis revealed that in the absence of scaffolds even after 3 months the lesions were covered with only a thin fibrous layer (Fig. 6A, B), mostly comprised of collagen. This is quite common in untreated defects of critical size[1] and is probably due to the lack of supporting tissue or scaffolding to allow cellular infiltration and tissue formation.[62] In a critical size defect, when large amounts of bone are removed during injury or surgery, the periosteum is no longer intact and does not have the ability to functionally restore the area.[23] Based on our results, we posit that mineralized CTS-GP scaffolds may serve as bridging templates to initiate integration with the surrounding tissue and facilitate tissue ingrowth from the periphery of the defects. Indeed, as seen in Figure 6C and E, most of the tissue formation occurs from the periphery. We speculate that due to their unique topography, electrospun scaffolds (thin membrane-like scaffolds, rather than foam fillers, metal implants, etc.) will readily integrate with the outer surface of the bone and stimulate the periosteum to initiate wound healing. As seen in Figure 6D and F, there was significant collagen formation, along the outer edge of the scaffold that appeared to be emanating from the outer edge of the cortical surface, as inferred from the pattern of the MTS stains.

Taken together, by enabling both cellular infiltration and ECM deposition, our composite CTS-HA-GP scaffolds promote peripheral healing not seen in defects treated with the nonmineralized CTS-GP scaffolds. On the other hand, the trade-off in using thin electrospun scaffolds is the limited penetration of cells into the scaffolds and tissues lack of tissue ingrowth into the scaffolds (Fig. 6C–F). From the histological data it is evident that there is new tissue formation at the periphery and along the surface of the implants, however, little ingrowth is observed completely penetrating the scaffold. This is a common issue with electrospun scaffolds and we, like many others, are looking into various ways of enhancing the porosity to elicit tissue ingrowth and cell penetration while still maintaining the integrity of the overall scaffold and the innate ECM-mimicking properties at the micro-level.[63–66]

Importantly, similar levels of new bone formation were observed at the peripheral edges of the CTS-HA-GP scaffolds with and without mMSCs, indicative of regenerative host/scaffold interactions.[26] It is well known that the periosteum harbors osteoprogenitor cells within the cambium layer, which are responsible for initiating bone healing.[21] Permissive electrospun biomaterials, like the ones used in our study, may be suitable to promote a periosteal response. Since mineralized CTS-HA-GP scaffolds without cells were equally effective in inducing host tissue ingrowth as were scaffolds with cells, we suggest that HA may act as nucleation sites, creating biochemical cues that can initiate osseointegration, facilitate healing responses, and promote tissue regeneration in critical size bone defects.

Acknowledgments

This study was supported, in part, by a grant from the National Science Foundation [grant # 0434108]. The authors are grateful to Dr. Gozde Senel for her help with the SEM, Dr. Darwin Prokop from the Institute of Regenerative Medicine at Texas A&M University for his generous gift of the mMSCs used for this study, and Drs. Anant Chopra and Yasha Kresh for the use of the Z1 Observer Zeiss microscope for fluorescent imaging. P.I.L. is the Laura H. Carnell Professor of Bioengineering, College of Engineering, Temple University.

Disclosure Statement

No other competing financial interests exist.

References

1. Cooper, G.M., Mooney, M.P., Gosain, A.K., Campbell, P.G., Losee, J.E., and Huard, J. Testing the critical size in calvarial bone defects: revisiting the concept of a critical-size defect. Plast Reconstr Surg **125,** 1685, 2010.
2. Senagore, A.J. The Gale encyclopedia of surgery: a guide for patients and caregivers. Detroit: Gale, 2004.
3. Laurie, S.W., Kaban, L.B., Mulliken, J.B., and Murray, J.E. Donor-site morbidity after harvesting rib and iliac bone. Plast Reconstr Surg **73,** 933, 1984.
4. Kurz, L.T., Garfin, S.R., and Booth, R.E., Jr. Harvesting autogenous iliac bone grafts. A review of complications and techniques. Spine (Phila Pa 1976) **14,** 1324, 1989.
5. Bhumiratana, S., and Vunjak-Novakovic, G. Concise review: personalized human bone grafts for reconstructing head and face. Stem Cell Transl Med **1,** 64, 2012.
6. Cooper, L.F. Biologic determinants of bone formation for osseointegration: clues for future clinical improvements. J Prosthet Dent **80,** 439, 1998.
7. Ripamonti, U. The induction of bone in osteogenic composites of bone matrix and porous hydroxyapatite replicas: an experimental study on the baboon (*Papio ursinus*). J Oral Maxillofac Surg **49,** 817, 1991.
8. Lykins, C.L., Friedman, C.D., Costantino, P.D., and Horioglu, R. Hydroxyapatite cement in craniofacial skeletal reconstruction and its effects on the developing craniofacial skeleton. Arch Otolaryngol Head Neck Surg **124,** 153, 1998.
9. Lee, D.W., Kim, J.Y., and Lew, D.H. Use of rapidly hardening hydroxyapatite cement for facial contouring surgery. J Craniofac Surg **21,** 1084, 2010.
10. Kumaran, S.T., Arun, K.V., Sudarsan, S., Talwar, A., and Srinivasan, N. Osteoblast response to commercially available demineralized bone matrices—an *in-vitro* study. Indian J Dent Res **21,** 3, 2010.
11. Zhang, W., Chen, J.L., Tao, J.D., Jiang, Y.Z., Hu, C.C., Huang, L., Ji, J.F., and Ouyang, H.W. The use of type 1 collagen scaffold containing stromal cell-derived factor-1 to create a matrix environment conducive to partial-thickness cartilage defects repair. Biomaterials **34,** 713, 2013.

12. Wolf-Brandstetter, C., Roessler, S., Storch, S., Hempel, U., Gbureck, U., Nies, B., Bierbaum, S., and Scharnweber, D. Physicochemical and cell biological characterization of PMMA bone cements modified with additives to increase bioactivity. J Biomed Mater Res B Appl Biomater **4,** 599, 2012.
13. Xie, X.H., Wang, X.L., Zhang, G., He, Y.X., Leng, Y., Tang, T.T., Pan, X., and Qin, L. Biofabrication of a PLGA-TCP-based porous bioactive bone substitute with sustained release of icaritin. J Tissue Eng Regen Med 2012. DOI: 10.1002/term.1679.
14. Mohammadi, Y., Soleimani, M., Fallahi-Sichani, M., Gazme, A., Haddadi-Asl, V., Arefian, E., Kiani, J., Moradi, R., Atashi, A., and Ahmadbeigi, N. Nanofibrous poly(epsilon-caprolactone)/poly(vinyl alcohol)/chitosan hybrid scaffolds for bone tissue engineering using mesenchymal stem cells. Int J Artif Organs **30,** 204, 2007.
15. Phipps, M.C., Clem, W.C., Grunda, J.M., Clines, G.A., and Bellis, S.L. Increasing the pore sizes of bone-mimetic electrospun scaffolds comprised of polycaprolactone, collagen I and hydroxyapatite to enhance cell infiltration. Biomaterials **33,** 524, 2012.
16. Cai, Y.Z., Wang, L.L., Cai, H.X., Qi, Y.Y., Zou, X.H., and Ouyang, H.W. Electrospun nanofibrous matrix improves the regeneration of dense cortical bone. J Biomed Mater Res A **95,** 49, 2010.
17. Frohbergh, M.E., Katsman, A., Botta, G.P., Lazarovici, P., Schauer, C.L., Wegst, U.G., and Lelkes, P.I. Electrospun hydroxyapatite-containing chitosan nanofibers crosslinked with genipin for bone tissue engineering. Biomaterials **33,** 9167, 2012.
18. Bavariya, A.J., Andrew Norowski, P., Jr., Mark Anderson, K., Adatrow, P.C., Garcia-Godoy, F., Stein, S.H., and Bumgardner, J.D. Evaluation of biocompatibility and degradation of chitosan nanofiber membrane crosslinked with genipin. J Biomed Mater Res B Appl Biomater **102,** 1084, 2014.
19. Norowski, P.A., Jr., Fujiwara, T., Clem, W.C., Adatrow, P.C., Eckstein, E.C., Haggard, W.O., and Bumgardner, J.D. Novel naturally crosslinked electrospun nanofibrous chitosan mats for guided bone regeneration membranes: material characterization and cytocompatibility. J Tissue Eng Regen Med 2012. DOI: 10.1002/term.1648.
20. De Bari, C., Dell'Accio, F., Vanlauwe, J., Eyckmans, J., Khan, I.M., Archer, C.W., Jones, E.A., McGonagle, D., Mitsiadis, T.A., Pitzalis, C., and Luyten, F.P. Mesenchymal multipotency of adult human periosteal cells demonstrated by single-cell lineage analysis. Arthritis Rheum **54,** 1209, 2006.
21. Hutmacher, D.W., Sittinger, M. Periosteal cells in bone tissue engineering. Tissue Eng **9 Suppl 1,** S45, 2003.
22. Ouyang, H.W., Cao, T., Zou, X.H., Heng, B.C., Wang, L.L., Song, X.H., and Huang, H.F. Mesenchymal stem cell sheets revitalize nonviable dense grafts: implications for repair of large-bone and tendon defects. Transplantation **82,** 170, 2006.
23. Zhang, X., Xie, C., Lin, A.S., Ito, H., Awad, H., Lieberman, J.R., Rubery, P.T., Schwarz, E.M., O'Keefe, R.J., and Guldberg, R.E. Periosteal progenitor cell fate in segmental cortical bone graft transplantations: implications for functional tissue engineering. J Bone Miner Res **20,** 2124, 2005.
24. Tawonsawatruk, T., Spadaccino, A., Murray, I.R., Peault, B., and Simpson, H.A. Growth kinetics of rat mesenchymal stem cells from 3 potential sources: bone marrow, periosteum and adipose tissue. J Med Assoc Thai **95 Suppl 10,** S189, 2012.
25. Xie, C., Reynolds, D., Awad, H., Rubery, P.T., Pelled, G., Gazit, D., Guldberg, R.E., Schwarz, E.M., O'Keefe, R.J., and Zhang, X. Structural bone allograft combined with genetically engineered mesenchymal stem cells as a novel platform for bone tissue engineering. Tissue Eng **13,** 435, 2007.
26. Hoffman, M.D., and Benoit, D.S. Emerging ideas: engineering the periosteum: revitalizing allografts by mimicking autograft healing. Clin Orthop Relat Res **471,** 721, 2012.
27. Hsieh, H.J., Hsieh, C.Y., Tsai, S.P., Ho, M.H., Wang, D.M., Liu, C.E., Hsieh, C.H., and Tseng, H.C. Analysis of freeze-gelation and cross-linking processes for preparing porous chitosan scaffolds. Carbohyd Polym **67,** 124, 2007.
28. Grassel, S., Stockl, S., and Jenei-Lanzl, Z. Isolation, culture, and osteogenic/chondrogenic differentiation of bone marrow-derived mesenchymal stem cells. Methods Mol Biol **879,** 203, 2012.
29. Lelkes, P.I., Samet, M.M., Christensen, C.W., and Amrani, D.L. Factitious angiogenesis: endothelialization of artificial cardiovascular prostheses. In: Maragoudakis, M.E., Gullino, P.M., and Lelkes, P.I., eds. Angiogenesis in Health and Disease. New York: Plenum Press, 1992, pp. 339–351.
30. Han, J., Lazarovici, P., Pomerantz, C., Chen, X., Wei, Y., and Lelkes, P.I. Co-electrospun blends of PLGA, gelatin, and elastin as potential nonthrombogenic scaffolds for vascular tissue engineering. Biomacromolecules **12,** 399, 2010.
31. O'Brien, J., Wilson, I., Orton, T., and Pognan, F. Investigation of the Alamar Blue (resazurin) fluorescent dye for the assessment of mammalian cell cytotoxicity. Eur J Biochem **267,** 5421, 2000.
32. Zhang, Y., Reddy, V.J., Wong, S.Y., Li, X., Su, B., Ramakrishna, S., and Lim, C.T. Enhanced biomineralization in osteoblasts on a novel electrospun biocomposite nanofibrous substrate of hydroxyapatite/collagen/chitosan. Tissue Eng Part A **16,** 1949, 2010.
33. Li, M., Mondrinos, M.J., Gandhi, M.R., Ko, F.K., Weiss, A.S., and Lelkes, P.I. Electrospun protein fibers as matrices for tissue engineering. Biomaterials **26,** 5999, 2005.
34. Im, J.Y., Min, W.K., You, C., Kim, H.O., Jin, H.K., and Bae, J.S. Bone regeneration of mouse critical-sized calvarial defects with human mesenchymal stem cells in scaffold. Lab Anim Res **29,** 196, 2013.
35. Lee, J.H., Lee, Y.J., Cho, H.J., and Shin, H. Guidance of in vitro migration of human mesenchymal stem cells and *in vivo* guided bone regeneration using aligned electrospun fibers. Tissue Eng Part A **20,** 2031, 2014.
36. Moore, K.A., and Lemischka, I.R. Stem cells and their niches. Science **311,** 1880, 2006.
37. Mandal, B.B., and Kundu, S.C. Cell proliferation and migration in silk fibroin 3D scaffolds. Biomaterials **30,** 2956, 2009.
38. Liu, X., Smith, L.A., Hu, J., and Ma, P.X. Biomimetic nanofibrous gelatin/apatite composite scaffolds for bone tissue engineering. Biomaterials **30,** 2252, 2009.
39. Holzwarth, J.M., and Ma, P.X. Biomimetic nanofibrous scaffolds for bone tissue engineering. Biomaterials **32,** 9622, 2011.
40. Ghasemi-Mobarakeh, L., Prabhakaran, M.P., Balasubramanian, P., Jin, G., Valipouri, A., and Ramakrishna, S.

Advances in electrospun nanofibers for bone and cartilage regeneration. J Nanosci Nanotechnol **13,** 4656, 2013.
41. Liu, H., Peng, H., Wu, Y., Zhang, C., Cai, Y., Xu, G., Li, Q., Chen, X., Ji, J., Zhang, Y., and OuYang, H.W. The promotion of bone regeneration by nanofibrous hydroxyapatite/chitosan scaffolds by effects on integrin-BMP/Smad signaling pathway in BMSCs. Biomaterials **34,** 4404, 2013.
42. Peng, H., Yin, Z., Liu, H., Chen, X., Feng, B., Yuan, H., Su, B., Ouyang, H., and Zhang, Y. Electrospun biomimetic scaffold of hydroxyapatite/chitosan supports enhanced osteogenic differentiation of mMSCs. Nanotechnology **23,** 485102, 2012.
43. Tchemtchoua, V.T., Atanasova, G., Aqil, A., Filee, P., Garbacki, N., Vanhooteghem, O., Deroanne, C., Noel, A., Jerome, C., Nusgens, B., Poumay, Y., and Colige, A. Development of a chitosan nanofibrillar scaffold for skin repair and regeneration. Biomacromolecules **12,** 3194, 2011.
44. Martins, A., Pinho, E.D., Correlo, V.M., Faria, S., Marques, A.P., Reis, R.L., and Neves, N.M. Biodegradable nanofibers-reinforced microfibrous composite scaffolds for bone tissue engineering. Tissue Eng Part A **16,** 3599, 2010.
45. Stoddart, M.J. Mammalian Cell Viability: Methods and Protocols. New York: Humana Press/Springer, 2011.
46. Birket, M.J., Orr, A.L., Gerencser, A.A., Madden, D.T., Vitelli, C., Swistowski, A., Brand, M.D., and Zeng, X. A reduction in ATP demand and mitochondrial activity with neural differentiation of human embryonic stem cells. J Cell Sci **124,** 348, 2011.
47. Kaji, H. [Pyrophosphate and mineralization (TNSALP, PC-1, ANK)]. Clin Calcium **17,** 1574, 2007.
48. Shafiee, A., Seyedjafari, E., Soleimani, M., Ahmadbeigi, N., Dinarvand, P., and Ghaemi, N. A comparison between osteogenic differentiation of human unrestricted somatic stem cells and mesenchymal stem cells from bone marrow and adipose tissue. Biotechnol Lett **33,** 1257, 2011.
49. Hu, Z., Peel, S.A., Lindholm, T.C., Sandor, G.K., Clokie, C.M., and Su, Y. Osteoinductivity of partially purified bovine, ostrich and emu bone morphogenetic proteins *in vitro*. J Biomed Mater Res A **98,** 473, 2011.
50. Hoemann, C.D., El-Gabalawy, H., and McKee, M.D. *In vitro* osteogenesis assays: influence of the primary cell source on alkaline phosphatase activity and mineralization. Pathol Biol (Paris) **57,** 318, 2009.
51. Wang, G., Liu, X., Zreiqat, H., and Ding, C. Enhanced effects of nano-scale topography on the bioactivity and osteoblast behaviors of micron rough ZrO2 coatings. Colloids Surf B Biointerfaces **86,** 267, 2011.
52. Acharya, C., Adesida, A., Zajac, P., Mumme, M., Riesle, J., Martin, I., and Barbero, A. Enhanced chondrocyte proliferation and mesenchymal stromal cells chondrogenesis in coculture pellets mediate improved cartilage formation. J Cell Physiol **227,** 88, 2012.
53. Erickson, I.E., Kestle, S.R., Zellars, K.H., Farrell, M.J., Kim, M., Burdick, J.A., and Mauck, R.L. High mesenchymal stem cell seeding densities in hyaluronic acid hydrogels produce engineered cartilage with native tissue properties. Acta Biomater **8,** 3027, 2012.
54. Menard, C., and Tarte, K. Immunoregulatory properties of clinical grade mesenchymal stromal cells: evidence, uncertainties, and clinical application. Stem Cell Res Ther **4,** 64, 2013.
55. Kang, Y.M., Lee, B.N., Ko, J.H., Kim, G.H., Kang, K.N., Kim da, Y., Kim, J.H., Park, Y.H., Chun, H.J., Kim, C.H., and Kim, M.S. *In vivo* biocompatibility study of electrospun chitosan microfiber for tissue engineering. Int J Mol Sci **11,** 4140, 2010.
56. Casiraghi, F., Perico, N., and Remuzzi, G. Mesenchymal stromal cells to promote solid organ transplantation tolerance. Curr Opin Organ Transplant **18,** 51, 2013.
57. Zimmermann, C.E., Gierloff, M., Hedderich, J., Acil, Y., Wiltfang, J., and Terheyden, H. Survival of transplanted rat bone marrow-derived osteogenic stem cells *in vivo*. Tissue Eng Part A **17,** 1147, 2011.
58. Zhu, H.Y., Yu, D., Zhou, Y., Wang, C., Gao, M.F., Jiang, H.L., and Wang, H.M. Biological activity of a nanofibrous barrier membrane containing bone morphogenetic protein formed by core-shell electrospinning as a sustained delivery vehicle. J Biomed Mater Res B **101B,** 541, 2013.
59. Lee, Y.J., Lee, J.H., Cho, H.J., Kim, H.K., Yoon, T.R., and Shin, H. Electrospun fibers immobilized with bone forming peptide-1 derived from BMP7 for guided bone regeneration. Biomaterials **34,** 5059, 2013.
60. Schofer, M.D., Roessler, P.P., Schaefer, J., Theisen, C., Schlimme, S., Heverhagen, J.T., Voelker, M., Dersch, R., Agarwal, S., Fuchs-Winkelmann, S., and Paletta, J.R.J. Electrospun PLLA nanofiber scaffolds and their use in combination with BMP-2 for reconstruction of bone defects. PLoS One **6,** 2011.
61. Son, S.R., Linh, N.T.B., Yang, H.M., and Lee, B.T. *In vitro* and *in vivo* evaluation of electrospun PCL/PMMA fibrous scaffolds for bone regeneration. Sci Technol Adv Mat **14,** 2013.
62. Zhang, X., Awad, H.A., O'Keefe, R.J., Guldberg, R.E., and Schwarz, E.M. A perspective: engineering periosteum for structural bone graft healing. Clin Orthop Relat Res **466,** 1777, 2008.
63. Nam, J., Huang, Y., Agarwal, S., and Lannutti, J. Improved cellular infiltration in electrospun fiber via engineered porosity. Tissue Eng **13,** 2249, 2007.
64. Baker, B.M., Gee, A.O., Metter, R.B., Nathan, A.S., Marklein, R.A., Burdick, J.A., and Mauck, R.L. The potential to improve cell infiltration in composite fiber-aligned electrospun scaffolds by the selective removal of sacrificial fibers. Biomaterials **29,** 2348, 2008.
65. Kim, T.G., Chung, H.J., and Park, T.G. Macroporous and nanofibrous hyaluronic acid/collagen hybrid scaffold fabricated by concurrent electrospinning and deposition/leaching of salt particles. Acta Biomater **4,** 1611, 2008.
66. Skotak, M., Ragusa, J., Gonzalez, D., and Subramanian, A. Improved cellular infiltration into nanofibrous electrospun cross-linked gelatin scaffolds templated with micrometer-sized polyethylene glycol fibers. Biomed Mater **6,** 055012, 2011.

Address correspondence to:
Peter I. Lelkes, PhD
Department of Bioengineering
College of Engineering
Temple University
Engineering Building Room 811
1947 North 12th Street
Philadelphia, PA 19122

E-mail: pilelkes@temple.edu

Received: December 31, 2013
Accepted: October 6, 2014
Online Publication Date: December 11, 2014